Preparation of hexagonal plate $Na_xCoO_\alpha \cdot nH_2O$ crystals via the thermal decomposition of sodium hexanitrocobaltate (III) and their properties

Susumu Nakayama (Department of Applied Chemistry and Biotechnology, National Institute of Technology (KOSEN), Niihama College, s.nakayama@niihama-nct.ac.jp, Japan)

Abstract

Na_xCoO_2 is a widely used cathode material for sodium-ion batteries, which are expected to replace lithium-ion batteries. In this study, $Na_xCoO_\alpha \cdot nH_2O$ crystals were prepared from $Na_3[Co(NO_2)_6]$ using a complex pyrolysis method. According to thermogravimetric (TG)–differential thermal analysis results, $Na_3[Co^{III}(NO_2)_6]$ was pyrolyzed into a mixture of $NaNO_3$, Na_2O, and $Co^{II,III}{}_3O_4$ at 250-350 °C and Na_2O and $NaCo^{II,III}O_{1.83}$ above 800 °C. It was found that $Na_3[Co(NO_2)_6]$ existed in the form of thin Co-rich hexagonal platelet crystals embedded into Na-rich or amorphous crystals after heat treatment at 700 °C for 2 h. After further washing with deionized water, only the thin hexagonal platelet crystals were observed, whereas the Na-rich or amorphous crystals disappeared. X-ray diffraction measurements revealed that the hexagonal platelet crystals consisted of a single γ-Na_xCoO_2 phase. Its chemical composition estimated via energy-dispersive X-ray spectroscopy and TG analysis was $Na_{0.34}CoO_{1.39} \cdot 0.20H_2O$. The intragranular and intergranular resistivities of $Na_{0.34}CoO_{1.39} \cdot 0.20H_2O$ crystals compressed at 100 MPa were 200 and 80 Ω·cm, respectively, at room temperature. Furthermore, $Na_{0.34}CoO_{1.39} \cdot 0.20H_2O$ powder can be potentially used as a positive electrode in Na-ion batteries.

Key words
TG-DTA, SEM-EDS, Nyquist plot, cathode, charge/discharge

1. Introduction

Lithium-ion batteries, which are widely used as large-scale secondary batteries for storing natural energy such as solar and wind power, are the most promising energy storage devices because of their high charge–discharge efficiency. However, as lithium-ion batteries have become widespread and larger in size, maintaining the stable supply of lithium as well as rare metals such as cobalt (used as an electrode material) is an important task because high-grade lithium resources are ubiquitous in the region with the largest concentration in South America. Meanwhile, sodium-ion batteries have been identified as a post-lithium-ion batteries, and their extensive studies have brought them closer to practical utilization (Cai et al., 2024; Azambou et al., 2024). Sodium is more abundant and less expensive than lithium, a homologous element, rendering it an element with a stable supply. However, the key issue with these batteries is that the ionic radius of the six-coordinated Na^+ ion (1.02 Å) is larger than that of the six-coordinated Li^+ ion (0.74 Å) (Shannon and Prewitt, 1969). This leads to an irreversible structural collapse of the electrode material, resulting in significant capacity loss (Luo et al., 2016). Recently, the layered transition metal oxide Na_xCoO_2 ($0 < x < 1$), with a structure analogous to that of LiCoO2 (used as a cathode material in lithium-ion batteries), has garnered considerable attention due to its high energy density and unexpected cycle stability (Rai et al., 2014; Gao et al., 2018; Kehne et al., 2019). It is often prepared by a solid-state reaction method, in which the precursors, Co_3O_4 and Na_2CO_3, are heat-treated at 700-900 °C. Recently, sol-gel and hydrothermal approaches to Na_xCoO_2 ($0 < x < 1$) synthesis have also been reported, with detailed physicochemical investigations. For example, Gao et al. synthesized self-supported $Na_{0.7}CoO_2$ nanosheet arrays via a facile "sodiation and post-calcination" method to improve the active material utilization (Gao et al., 2016). In another study, they synthesized P2-type Na_xCoO_2 microspheres by this novel strategy and investigated their electrochemical performance (Gao et al., 2020). Kalaimathi and Babu employed a sol-gel method to prepare layered Na_xCoO_2 ($x = 1, 0.9, 0.7, 0.5, 0.3, 0.1$) from $NaNO_3$ and $Co(NO_3)_2 \cdot 6H_2O$, and comprehensively investigated its structural, electronic, optical, and electrical properties (Kalaimathi and Babu, 2024). Na_xCoO_2 is also employed as a thermoelectric conversion material (Nagira et al., 2023), and $Na_xCoO_2 \cdot 1.3H_2O$—as a superconducting material (Schaak et al., 2003). Na_xCoO_2 powders are frequently prepared by a solid phase reaction method, in which Co_3O_4 and Na_2CO_3 are used as the starting materials and heat-treated at 700-900 °C (Rai et al., 2014; Kehne et al., 2019; Nagira et al., 2023). Other reported cases include the preparation of Na_xCoO_2 crystals with dimensions of $4 \times 4 \times 0.5$ mm^3 via a flux method using NaOH and Co_3O_4 as the starting materials and Na_xCoO_2 thin film via pulsed laser deposition (Wang et al., 2005; Hildebrandt et al., 2013).

In this study, we focused on the preparation of $Na_xCoO_\alpha \cdot nH_2O$ crystals through the thermal decomposition of sodium hexanitrocobalt (III) ($Na_3[Co(NO_2)_6]$) complex. Compared with the solid-phase reaction and coprecipitation methods, in complex oxides prepared via the thermal decomposition of complexes containing multiple metal elements, such elements are uniformly dispersed at the atomic level (Nakayama, 2001; Nakayama et al., 2003). Because $Na_3[Co(NO_2)_6]$ contains three moles of Na per one mole of Co, we assumed that it included the elements utilized in the flux method and could form large crystals.

2. Experimental procedure

2.1 Sample preparation

Sodium hexanitrocobalt (III) ($Na_3[Co(NO_2)_6]$) reagent was procured from Fujifilm Wako Pure Chemicals Co. First, 10 g of $Na_3[Co(NO_2)_6]$ was packed in an alumina crucible (Nikkato Co., SSA-S) and heat-treated at 700 °C for 2 h. The resulting material was washed with deionized water (approximately 150 times excess by weight) while stirring for 10 min, filtered by suction, and dried at 100 °C to obtain a heat-treated deionized water-washed sample, labelled as $Na_xCoO_\alpha \cdot nH_2O$.

2.2 Fabrication of an all-solid-state Na-ion battery

The Na-ion batteries employing the prepared $Na_xCoO_\alpha \cdot nH_2O$ samples as positive electrode materials were fabricated in an air atmosphere. Polyvinyl alcohol (PVA; degree of saponification: 78-82 mol%, average degree of polymerization: 1,500–1,800) and lithium nitrate $NaNO_3$ (99.9 %) were obtained from Fujifilm Wako Pure Chemicals Co. Hard carbon black (HC, JCP-P64) was manufactured by JFE Chemical Co. A 10 % PVA solution was prepared by dissolving PVA in deionized water at 80 °C. A 30 % $NaNO_3$–PVA solution was produced by mixing 50 mL of 10% PVA with a solution of 2.0 g $NaNO_3$ dissolved in 10 mL of deionized water at room temperature. The 30% $NaNO_3$–PVA solution was placed in a polyethylene Petri dish with an inner diameter of 30 mm and dried and solidified at 60 °C on a hot plate to produce 30% $NaNO_3$–PVA electrolyte sheets. The negative and positive electrodes were fabricated as follows: 0.1 g of HC was thoroughly mixed with 1.0 mL of the 30 % $NaNO_3$–PVA solution in an agate mortar, applied to one side of the 30 % $NaNO_3$–PVA electrolyte sheet using a spatula, and dried at 60 °C on a hot plate. Next, 0.16 mg of $Na_xCoO_\alpha \cdot nH_2O$, 0.1 g of HC, and 1.0 mL of the 30 % $NaNO_3$–PVA solution were thoroughly mixed in an agate mortar, applied to the other side of the 30 % $NaNO_3$–PVA electrolyte sheet using a spatula, and fixed by drying at 60 °C on a hot plate.

2.3 Characterization

2.3.1 Physicochemical analysis

$Na_3[Co(NO_2)_6]$ was packed in 10 mg of platinum pans, and thermogravimetric differential thermal analysis (TG–DTA, Rigaku Co., TG8120) measurements were performed in a temperature range from room temperature to 900 °C (heating rate: 10 $°C \cdot min^{-1}$) in an air stream with a flow rate of 20 $mL \cdot min^{-1}$. X-ray diffraction (XRD, Rigaku Co., MiniFlex II) was performed in the range of 2θ = 10-80° using CuK_α radiation. For analytical electron microscopy observations, each sample was platinum-coated with an ion coater (JEOL Ltd., JEC-1600). Morphological observations were performed via field-emission scanning electron microscopy (FE–SEM, JEOL Ltd., JSM-7500F). Elemental analysis was conducted using an energy-dispersive X-ray spectroscopy (EDS) analyzer (JEOL Ltd., JED-2300) attached to the FE–SEM instrument. The acceleration voltage and irradiation current utilized for observations and elemental analyses were 20 kV and 1.0 nA, respectively.

The ionic conductivity of the $Na_xCoO_\alpha \cdot nH_2O$ sample was measured at room temperature in air with an impedance meter (HP4194) at frequencies ranging from 100 Hz to 10 MHz. A constant pressure of 100 MPa was applied to the sample powder using a uniaxial press, with an alumina ceramic mold and stainless-steel electrodes. Complex impedance analysis was then performed on the acquired data.

2.3.2 Charge–discharge measurements

The all-solid-state Na-ion battery with the negative and positive electrodes formed on both sides of the prepared $NaNO_3$–PVA electrolyte sheet was sandwiched between stainless-steel measuring fixtures (electrodes, φ15 mm), and its characteristics were measured using a DC voltage and current source–monitor (ADC Co., 6242) in air atmosphere. Its DC resistance was measured using a digital multimeter (ADC Co., 7355).

3. Results and discussion

3.1 Pyrolysis behavior of $Na_3[Co(NO_2)_6]$

The TG–DTA results obtained for $Na_3[Co^{III}(NO_2)_6]$ and the XRD patterns of its thermal decomposition products are shown in Figure 1 and 2, respectively. The XRD pattern (Figure 2 (a)) reveals that the precursor ($Na_3[Co^{III}(NO_2)_6]$) exists in a single phase. Figure 1 shows that a large weight loss with an endothermic peak is observed at approximately 200 °C. An XRD pattern of the sample after the heat treatment at 250 °C for 2 h is shown in Figure 2 (b). It contains the peaks attributed to $NaNO_3$, Na_2O, and Co_3O_4. The theoretical weight loss during the pyrolysis of $Na_3[Co^{III}(NO_2)_6]$ into

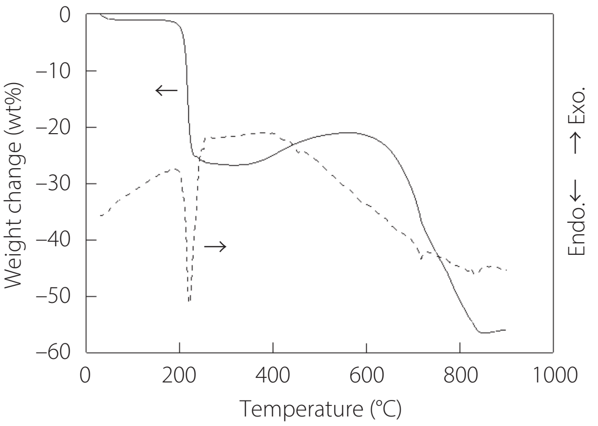

Figure 1: TG–DTA curves of $Na_3[Co(NO_2)_6]$

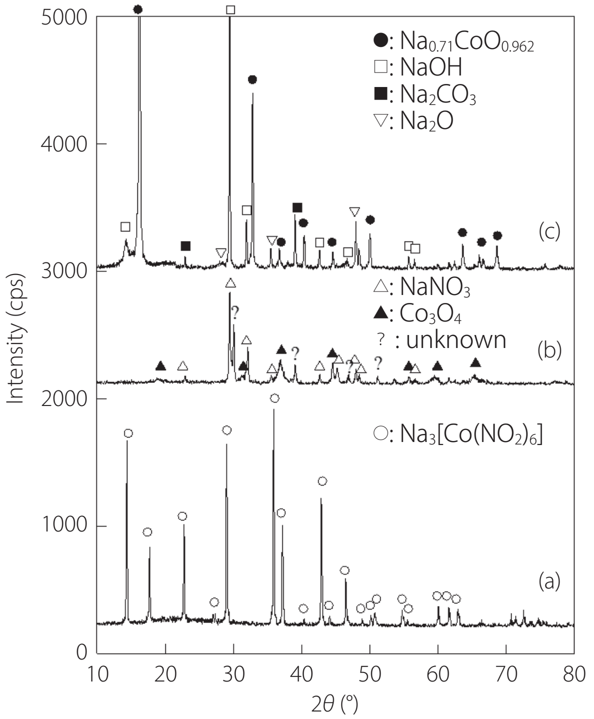

Figure 2: XRD patterns of (a) $Na_3[Co(NO_2)_6]$, (b) the sample heat-treated at 250 °C for 2 h, and (c) the sample heat-treated at 700 °C for 2 h

Note: ●: $Na_{0.71}CoO_{0.962}$ (ICDD No. 30-1182), ○: $Na_3[Co(NO_2)_6]$ (ICDD No. 29-1201), ▲: Co_3O_4 (ICDD No. 9-418), △: $NaNO_3$ (ICDD No. 36-1474), ■: Na_2CO_3 (ICDD No. 25-816), □: NaOH (ICDD No. 1-1173), and ▽: Na_2O (ICDD No. 3-1074).

$2NaNO_3 \cdot 1/2Na_2O \cdot 1/3Co^{II,III}{}_3O_4$ is 30.37 %, suggesting that a mixture of $NaNO_3$, Na_2O, and $Co^{II,III}{}_3O_4$ is formed in the plateau region (weight loss: approximately 27 %) between 250 and 350 °C. A weight increase is observed at 400-600 °C, which is likely due to the absorption of atmospheric CO_2 by molten $NaNO_3$. Subsequently, a large weight loss with an endothermic peak is observed around 700 °C, and a final plateau is reached above 800 °C. The weight loss at the final plateau is approximately 57 %. When $Na_3[Co^{III}(NO_2)_6]$ is heated at a rate of 10 $°C \cdot min^{-1}$ and subjected to an isothermal TG measurement at 700 °C for 1 h, the weight loss is approximately 57 %. This suggests that the heat-treated sample obtained, as reported in Section 2.1, is the same as the product formed in the final plateau region. The XRD pattern of this sample is shown in Figure 2 (c). It contains the peaks attributed to Na_2O, NaOH, Na_2CO_3, and Na_xCoO_α ($Na_{0.71}CoO_{0.962}$, ICDD No. 30-1182). NaOH and Na_2CO_3 are likely formed in air after the heat treatment at 700 °C. $Na_3[Co(NO_2)_6]$ is transformed to Na_2O and $NaCo^{II,III}O_{1.83}$, and the theoretical weight loss during the pyrolysis reaction is 57.11 %, suggesting that a mixture of Na_2O and $NaCo^{II,III}O_{1.83}$ is formed in the final plateau region (final product). The stable cobalt oxides are $Co^{II}O$ and $Co^{II,III}{}_3O_4$. $Co^{II,III}{}_3O_4$ is stable at 600-800 °C, and $Co^{II}O$ is formed above 900 °C (Greenwood and Earnshaw, 1997).

3.2 Morphologies of $Na_3[Co(NO_2)_6]$, heat-treated $Na_3[Co(NO_2)_6]$, and $Na_xCoO_\alpha \cdot nH_2O$

The reflected electron images of $Na_3[Co(NO_2)_6]$ reagent, the sample heat-treated at 700 °C for 2 h, and the sample washed with deionized water are shown in Figure 3. The $Na_3[Co(NO_2)_6]$ sample presented in Figure 3 (a) contains prismatic crystals with long sides of approximately 30 μm. The sample heat-treated at 700 °C for 2 h (Figure 3 (b)) consists of thin hexagonal plate-like crystals with lengths of approximately 10 μm embedded into other crystals or non-crystals. The reflected electron image contains bright thin hexagonal platelet-shaped crystals, suggesting the presence of a large Co amount. Meanwhile, the other (or amorphous) crystals exhibit a darker color, indicating the abundance of Na element. For the sample heat-treated at 700 °C for 2 h and then washed with deionized water (Figures 3 (c) and (d)), only thin hexagonal plate-like crystals with sides of approximately 10 μm are observed, and the Na-rich or amorphous crystals depicted in Figure 3 (b) have been likely removed by deionized water washing.

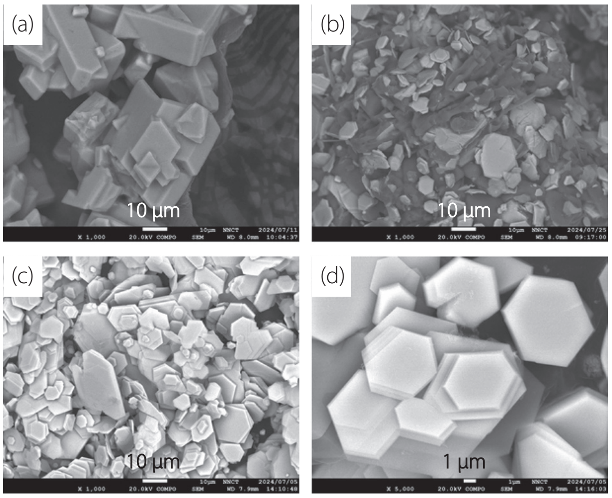

Figure 3: Reflected electron images (×1,000) of (a) $Na_3[Co(NO_2)_6]$, (b) the sample heat-treated at 700 °C for 2 h, (c) $Na_xCoO_\alpha \cdot nH_2O$, and (d) the sample depicted in panel (c) (magnification: × 5,000)

3.3 Elemental analyses of $Na_3[Co(NO_2)_6]$, heat-treated $Na_3[Co(NO_2)_6]$, and $Na_xCoO_\alpha \cdot nH_2O$

The EDS results of the samples are summarized in Table 1. For $Na_3[Co(NO_2)_6]$, the Na/Co atomic ratio is 1.25/1, N/Co atomic ratio is 2.47/1, and O/Co atomic ratio is 5.86/1. The $Na_3[Co(NO_2)_6]$ sample heat-treated at 700 °C for 2 h exhibits a Na/Co atomic ratio of 1.47/1, N/Co atomic ratio of 0.45/1, and O/Co atomic ratio of 4.87/1. Hence, the Na/Co atomic ratios determined for $Na_3[Co(NO_2)_6]$ and the sample heat-treated at 700 °C for 2 h are nearly identical. Meanwhile, the EDS results obtained for the $Na_xCoO_\alpha \cdot nH_2O$ sample show a Na/Co atomic

Table 1: EDS analysis results obtained for (a) $Na_3[Co(NO_2)_6]$, (b) the sample prepared by heat-treating $Na_3[Co^{III}(NO_2)_6]$ at 700 °C for 2 h, and (c) $Na_xCoO_\alpha{\cdot}nH_2O$

	atom %			
	N	O	Na	Co
(a)	28.43	59.10	9.73	2.74
(b)	–	78.95	16.64	4.41
(c)	–	64.93	9.26	25.81

ratio of 0.14/1 and O/Co atomic ratio of 0.68/1, indicating that the contents of Na and O atoms are extremely low. This phenomenon may be due to the removal of Na_2O, NaOH, and Na_2CO_3 species by deionized water washing, as confirmed by the XRD patterns depicted in Figure 2 (c). Note that deionized water washing was performed for 10, 30, and 60 min. The EDS results obtained for the three samples are nearly identical, indicating that the removal of Na_2O, NaOH, and Na_2CO_3 has been completed within 10 min. The composition (Na_xCoO_α) of hexagonal plate crystals in the sample heat-treated at 700 °C for 2 h and washed with deionized water is $Na_{0.34}CoO_{1.39}$, which is determined from the Na/Co atomic ratio of $Na_3[Co(NO_2)_6]$ equal to 1.25/1.

3.4 Crystal structure of the $Na_xCoO_\alpha{\cdot}nH_2O$ sample

The XRD pattern of the $Na_xCoO_\alpha{\cdot}nH_2O$ sample is shown in Figure 4. All peaks are consistent with the γ-Na_xCoO_2 structure ($Na_{0.71}CoO_{0.962}$, ICDD No. 30-1182) except for the broad peak at around 2θ = 19° (Wang et al., 2005; Kalaimathi and Babu, 2024). The peak intensities of the (002) and (004) planes are significantly higher than those of the respective peak intensities listed in ICDD No. 30-1182, indicating that the layered structure is oriented in the c-axis direction. Na_xCoO_α has three crystal structures: α-Na_xCoO_2 ($0.9 \le x \le 1$), β-Na_xCoO_2 ($0.55 \le x \le 0.6$), and γ-Na_xCoO_2 ($0.5 \le x \le 0.9$).

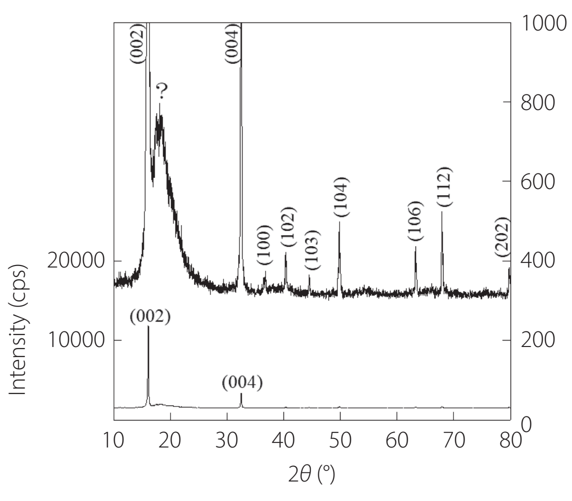

Figure 4: XRD pattern of the $Na_xCoO_\alpha{\cdot}nH_2O$ sample

Note: The numbers represent the Miller indexes of $Na_{0.71}CoO_{0.962}$ reported in ICDD No. 30-1182.

The possible presence of crystalline water due to water washing in the $Na_xCoO_\alpha{\cdot}nH_2O$ sample was analyzed via TG–DTA. A weight loss of approximately 5.9 % is observed at around 380 °C (Figure 5), attributed to the desorption of interlayer water from the Na_xCoO_α crystals, based on which its composition is estimated as $Na_{0.34}CoO_{1.39}{\cdot}0.20H_2O$. The crystalline water was desorbed via heat treatment at 400 °C or higher temperatures; however, it reabsorbed when the sample was placed in water again. The crystalline water also gradually returned when the sample was left in air after heat treatment.

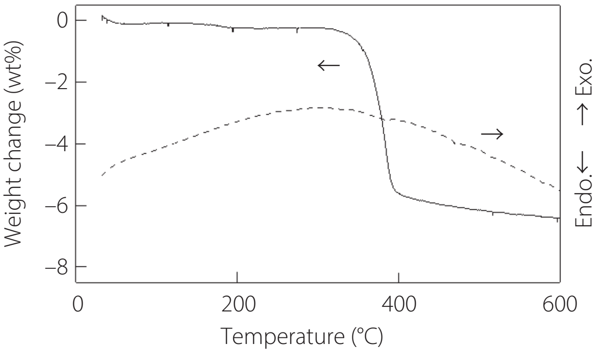

Figure 5: TG–DTA curves of the $Na_xCoO_\alpha{\cdot}nH_2O$ sample

3.5 Electrical properties of the $Na_xCoO_\alpha{\cdot}nH_2O$ sample

Figure 6 shows the room-temperature Nyquist plot of the $Na_{0.34}CoO_{1.39}{\cdot}0.20H_2O$ sample compressed at 100 MPa. Resistances that hinder ionic conduction in powder compacts include the intragranular resistance, grain boundary resistance, and electrode interface resistance, and the single arc presented in the Nyquist plot is likely due to the grain boundary resistance (R_{gb}). The Z′-axis value on the high-frequency side of the arc (left side of the Z′-axis) indicates the intragranular resistance (R_b), and the Z′-axis value on the low-frequency side of the arc (right side of the Z′-axis) corresponds to R_b +

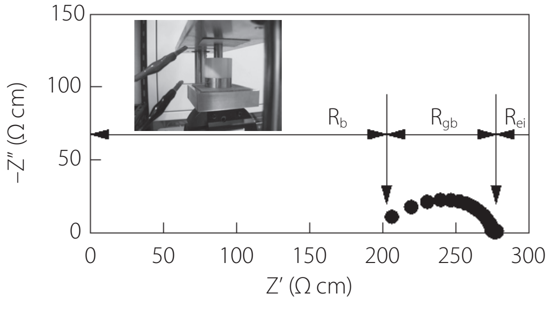

Figure 6: Nyquist plot the $Na_xCoO_\alpha{\cdot}nH_2O$ sample compressed at 100 MPa

Note: The inset depicts a digital photograph of the holder for the electrical measurement.

R_{gb}. The R_b magnitude obtained from the Z'-axis values is 200 Ω·cm, and R_{gb} = 80 Ω·cm. In addition, a slight increase (spike) of the arc caused by the electrode interface resistance (R_{ei}) between the piezoelectric material and electrode is observed on the low frequency side (right side of the Z'-axis).

3.6 Charge–discharge characteristics of the Na-ion battery using $Na_xCoO_α·nH_2O$ as the positive electrode material

Na-ion batteries were prepared using the $Na_xCoO_α·nH_2O$ samples as positive electrodes, and their charge–discharge characteristics were obtained (Nakayama, 2024). The results of constant-current charging conducted at 5.7 mA·cm^{-2} for 10 min and constant-current discharging conducted at 5.7 μA·cm^{-2} for 10 min in air at room temperature are shown in Figure 7. After approximately 10 min of charging, a voltage of 3.2 V is achieved, indicating successful charging. The results of discharging immediately after charging are shown in Figure 7. When a constant-current discharge process is initiated, the voltage at the start of the discharge process is 2.6 V, and a voltage drop of 0.8 V is observed; however, the discharge process continues thereafter, and the voltage after 10 min is 1.4 V. Hence, the $Na_xCoO_α·nH_2O$ sample can be employed as a positive electrode for Na-ion batteries. Because the voltage drop expected from the DC resistance (300 Ω) of the Na-ion battery measured with a multimeter is 0.002 V, the voltage drop of 0.8 V from 3.2 V at the end of charging to 2.6 V at the beginning of discharge is approximately 400 times greater than the calculated value. This effect is likely caused by the increase in the DC resistance due to the formation of products at the electrolyte/electrode interface during charging or rapid self-discharge immediately after charging; however, it has not been clarified in the present work.

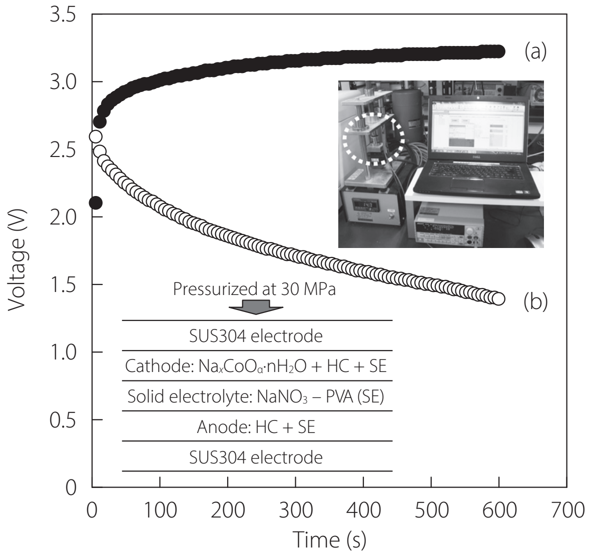

Figure 7: Voltage changes observed during (a) charging at 5.7 mA·cm^{-2} and (b) discharging at 5.7 μA·cm^{-2} for the integrated battery consisting of the ($Na_xCoO_α·nH_2O$–HC–30%$NaNO_3$–PVA) positive electrode/(30%$NaNO_3$–PVA) electrolyte/(HC–30%$NaNO_3$–PVA) negative electrode sheet. HC: hard carbon.

Notes: The inset (top) shows a digital photograph of the system used to evaluate the charge-discharge characteristics of the all-solid-state Na-ion battery. The inset (bottom) depicts the schematic of the charge–discharge evaluation setup for the all-solid-state Na-ion battery.

4. Conclusion

In this study, the physicochemical and electrochemical properties of $Na_xCoO_α·nH_2O$ prepared via the thermal decomposition of $Na_3[Co(NO_2)_6]$ were investigated. The obtained results are summarized below.

- According to the TG–DTA data, $Na_3[Co^{III}(NO_2)_6]$ formed a mixture of $NaNO_3$, Na_2O, and $Co^{II,III}{}_3O_4$ between 250-350 °C after a large weight loss with an endothermic peak was observed at around 200 °C followed by a large weight loss with an endothermic peak at around 700 °C and plateau above 800 °C. The final product contained a mixture of Na_2O and $NaCo^{II,III}O_{1.83}$.
- When $Na_3[Co(NO_2)_6]$ was heat-treated at 700 °C for 2 h, thin hexagonal platelet crystals with lengths of approximately 10 μm were embedded into other crystals. The reflected electron image contained bright hexagonal platelet crystals, indicating the presence of a large amount of Co, while the other crystals were dark, indicating the presence of a large amount of Na.
- When $Na_3[Co(NO_2)_6]$ was heat-treated at 700 °C for 2 h and then washed with deionized water, only thin hexagonal platelet crystals with sizes of approximately 10 μm were observed, and the other crystals with high Na contents disappeared after deionized water washing. The hexagonal platelet crystals consisted of a single γ-Na_xCoO_2 phase according to the XRD results. Furthermore, the peak intensities of the (002) and (004) planes were remarkably large. The TG results confirmed the presence of interlayer water, and the crystal composition was $Na_{0.34}CoO_{1.39}·0.20H_2O$.
- The intragranular and intergranular resistivities of the pressed powder heat-treated at 700 °C and then washed with deionized water were 200 and 80 Ω·cm at room temperature, respectively. This sample can be used as a positive electrode for Na-ion batteries.

The method for the preparation of $Na_xCoO_α·nH_2O$, as presented in this report, is simpler than conventional approaches, including solid-state reactions, and is considered superior due to the uniform atomic-level dispersion of Na and Co in the final product.

Acknowledgement

We would also like to thank JFE Chemical Corporation for supplying us with hard carbon black (JCP-P64) and Editage (www.editage.jp) for English language editing.

References

Azambou, C. I., Obiukwu, O. O., Tsobnang, P. K., Kenfack, I. T., Kalu, E. E., and Oguzie, E. E. (2024). Electrochemical performance and structural evolution of layered oxide cathodes materials for sodium-ion batteries: A review. *Journal of Energy Storage*, Vol. 94, 112506.

Cai, X., Yue, Y., Yi, Z., Liu, J., Sheng, Y., and Lu, Y. (2024). Challenges and industrial perspectives on the development of sodium ion batteries. *Nano Energy*, Vol. 129, 110052.

Gao, L., Chen, S., Zhang, L., and Yang, X. (2018). Self-supported $Na_{0.7}CoO_2$ nanosheet arrays as cathodes for high performance sodium ion batteries. *Journal of Power Sources*, Vol. 396, pp. 379-385.

Gao, L., Chen, S., Hu, H., Cheng, H., Zhang, L., and Yang, X. (2020). Hierarchical Na_xCoO_2 microspheres with low surface area toward high performance sodium ion batteries. *Materials Letters*, Vol. 260, 126965.

Greenwood, N. N. and Earnshaw, A. (1997). 26 Cobalt, Rhodium and Iridium. *Chemistry of the Elements (Second Edition)*, pp. 1113-1143.

Hildebrandt, S., Komissinskiy, P., Major, M., Donner, W., and Alff, L. (2013). Epitaxial growth and control of the sodium content in Na_xCoO_2 thin films. *Thin Solid Films*, Vol. 545, pp. 291-295.

Kalaimathi, S. and Babu, K. S. (2024). Enhancing electrical and optical properties in layered Na_xCoO_2 through sodium non-stoichiometry: Insights into surface band bending and oxygen vacancies. *Surfaces and Interfaces*, Vol. 47, 104208.

Kehne, P., Guhl, C., Alff, L., Hausbrand, R., and Komissinskiy, P. (2019). The effect of calcium impurities of β″-alumina on the degradation of Na_xCoO_2 cathodes in all solid state sodium-ion batteries. *Solid State Ionics*, Vol. 341, 115041.

Luo, W., Shen, F., Bommier, Zhu, C. H., Ji, X., and Hu, L. (2016). Na-ion battery anodes: Materials and electrochemistry. *Accounts of Chemical Research*, Vol. 49, pp. 231-240.

Nagira, T., Ito, M., Katsuyama, S., Majima, K., and Nagai, H. (2023). Thermoelectric properties of $(Na_{1-y}M_y)_xCo_2O_4$ (M=K, Sr, Y, Nd, Sm and Yb; y=0.01-0.35). *Journal of Alloys and Compounds*, Vol. 348, pp. 263-269.

Nakayama, S. (2001). $LaFeO_3$ perovskite-type oxide prepared by oxide-mixing, co-precipitation and complex synthesis methods. *Journal of Materials Science*, Vol. 36, pp. 5643-5648.

Nakayama, S., Okazaki, M., Aung, Y. L., and Sakamoto, M. (2003). Preparations of perovskite-type oxides $LaCoO_3$ from three different methods and their evaluation by homogeneity, sinterability and conductivity. *Solid State Ionics*, Vol. 158, pp. 133-139.

Nakayama, S, (2024). All-solid-state polyvinyl-alcohol-based Li-ion battery fabricated in air and its charge/discharge measurements. *Studies in Science and Technology*, Vol. 13, pp. 61-64.

Rai, A. K., Anh, L. T., Gim, J., Mathew, V., and Kim, J. (2014). Electrochemical properties of Na_xCoO_2 (x~0.71) cathode for rechargeable sodium-ion batteries. *Ceramics International*, Vol. 40, pp. 2411-2417.

Schaak, R. E., Klimczuk, T., Foo, M. L., and Cava, R. J. (2003). Superconductivity phase diagram of $Na_xCoO_2 \cdot 1.3H_2O$. *Nature*, Vol. 424, pp. 527-529.

Shannon, R. D. and Prewitt, C. T. (1969). Effective ionic radii in oxides and fluorides. *Acta Crystallographica B*, Vol. 25, pp. 925-946.

Wang, H., Chen, Z., and Jin, Q. (2005). Crystal growth and transport properties of α- and γ-phase Na_xCoO_2. *Materials Letters*, Vol. 59, pp. 3917-3920.

Received: March 31, 2025
Accepted: April 21, 2025
Published: June 30, 2025

https://doi.org/10.11425/sst.14.69